



Predictable and unpredictable modes of seasonal mean precipitation over Northeast China

Kairan Ying¹ · Carsten S. Frederiksen^{2,3} · Tianbao Zhao¹ · Xiaogu Zheng¹ ·
Zhe Xiong¹ · Xue Yi⁴ · Chunxiang Li¹

Received: 29 September 2016 / Accepted: 6 July 2017 / Published online: 13 July 2017
© Springer-Verlag GmbH Germany 2017

Abstract This study investigates the patterns of interannual variability that arise from the potentially predictable (slow) and unpredictable (intraseasonal) components of seasonal mean precipitation over Northeast (NE) China, using observations from a network of 162 meteorological stations for the period 1961–2014. A variance decomposition method is applied to identify the sources of predictability, as well as the sources of prediction uncertainty, for January–February–March (JFM), April–May–June (AMJ), July–August–September (JAS) and October–November–December (OND). The averaged potential predictability (ratio of slow to total variance) of NE China precipitation has the highest value of 0.32 during JAS and lowest value of 0.1 in AMJ. Possible sources of seasonal prediction for the leading predictable precipitation EOF modes come from the SST anomalies in the Japan Sea, as well as the North Atlantic during JFM, the Indian Ocean SST in AMJ, and the eastern tropical Pacific SST in JAS and OND. The prolonged linear trend, which is seen in the principal component time series of the leading predictable mode in JFM and OND, may also serve as a source of predictability. The Polar–Eurasia and Northern Annular Mode

atmospheric teleconnection patterns are closely connected with the leading and the second predictable mode of JAS, respectively. The Hadley cell circulation is closely related to the leading predictable mode of OND. The leading/second unpredictable precipitation modes for all these four seasons show a similar monopole/dipole structure, and can be largely attributed to the intraseasonal variabilities of the atmosphere.

Keywords Predictable signal · Unpredictable noise · Atlantic SST · Indian Ocean SST · ENSO · Atmospheric teleconnection

1 Introduction

Northeast (NE) China is a well-known grain producing and industrial base area. It is located in the mid-to-high latitudes of East Asia and is strongly affected by the East Asia monsoon (EAM) system (e.g. Ding 1992, 1994; Wang and Linho 2002). As a result, there has been a great deal of interest in the factors that influence the variability and predictability of NE China climate. Previous studies have found that there are a number of factors that are related to the interannual variability of seasonal precipitation in NE China. These include the sea surface temperatures (SSTs), Eurasian snow cover, soil moisture, and the atmospheric general circulation in both the extra-tropics and tropics (e.g. Yang et al. 2007a; Zhao et al. 2007; Liang et al. 2011; Gao et al. 2014a; Han et al. 2015). In particular, the internal dynamics of the atmospheric circulation systems, such as the northward migration of the western Pacific subtropical high (WPSH), the northern annular mode (NAM), and the blocking and the cold vortex, all play important roles in the climate variability of NE China (e.g. Sun et al.

✉ Carsten S. Frederiksen
C.Frederiksen@bom.gov.au

Zhe Xiong
xzh@tea.ac.cn

¹ CAS Key Laboratory of Regional Climate-Environment for Temperate East Asia, Institute of Atmospheric Physics, Chinese Academy of Sciences, Beijing, China

² The Bureau of Meteorology, Melbourne, Australia

³ The School of Earth, Atmosphere and Environment, Monash University, Clayton, VIC, Australia

⁴ Regional Climate Center of Shenyang, Shenyang, China

1994; He et al. 2006; Bueh et al. 2008; Shen et al. 2011). In addition, contemporary and/or lead–lag relationships between the interannual variation of NE China precipitation and SSTs over the eastern tropical Pacific Ocean (Wu et al. 2003; Zong et al. 2010; Gao et al. 2014b), the North Atlantic Ocean (Bai 2001; Zuo et al. 2013), and the Indian Ocean (Hu et al. 2003; Yang et al. 2007b; Gao et al. 2014a; Song and Zhou 2014) have been widely explored.

These many and varied factors result in the interannual variability of the seasonal mean precipitation over NE China having multiple time scales (intraseasonal, interannual, interdecadal, and longer) and a large spatial inhomogeneity (e.g. Jia et al. 2003; Tang et al. 2005; Gong et al. 2006). Our interest here is in the potential predictability of the seasonal mean precipitation, and the related precipitation patterns or modes. There is a limit for climate prediction, for example, the interannual variability of seasonal mean precipitation arising from the intraseasonal component is essentially unpredictable on seasonal or longer time scales. In the extra-tropics, in particular, a substantial component of interannual variability of seasonal mean fields arises from this variability within seasons (e.g. Zheng and Frederiksen 1999, 2004; Zheng et al. 2000; Frederiksen and Zheng 2004, 2007; Grainger et al. 2013, 2014; Ying et al. 2013, 2015, 2017). As a result, it is necessary to separate the interannual variability associated with the intraseasonal component from the total seasonal mean interannual variability to better identify and understand the more predictable signals and therefore possibly improving the seasonal forecasting of seasonal mean fields (Zheng and Frederiksen 2006; Zheng et al. 2008).

In order to examine the predictable and unpredictable patterns of seasonal mean fields separately, Zheng and Frederiksen (2004) developed a variance decomposition method (hereafter the “ZF2004 method”) able to estimate the interannual covariance matrices of the predictable (slow) and unpredictable (intraseasonal) components from monthly mean data. Specifically, the predictable patterns are more closely connected to the slowly varying external forcing and very low-frequency internal dynamics, such as the SSTs, sea-ice coverage and the equatorial stratospheric quasi-biennial oscillation; while the unpredictable patterns are associated with meteorological phenomena that vary significantly within a season, such as atmospheric blockings in the extra-tropics and the Madden–Julian Oscillation in the tropics. By separating out the weather noise, the predictable component will in general have a larger potential predictability than the total component, and a better relationships with the slow varying and persistent (interannual to supra-annual) processes.

In this study, we examine the predictable and unpredictable modes of seasonal precipitation over NE China, using the ZF2004 variance decomposition method. This

work extends the study of Ying et al. (2015, 2017), which identified the predictable signals of seasonal precipitation over eastern China (20° – 50° N, 95° – 135° E), an area strongly controlled by the EAM. However, as the precipitation variability in eastern China has its largest amplitude over the south, there are barely any loadings over NE China for the potentially predictable modes. Here, we focus on a smaller area of NE China, with the aim to better understand the temporal and spatial characteristics of the predictable signals and the sources of the predictability of NE China precipitation.

Following this introduction, the data and methodology are described in Sect. 2. The seasonal change and spatial pattern of the potential predictability are presented in Sect. 3.1; the potentially predictable modes and their associated SST and atmospheric circulation patterns are examined in Sect. 3.2; and the unpredictable precipitation modes are discussed in Sect. 3.3. Conclusion and discussion are given in Sect. 4.

2 Data and method

2.1 Data

The monthly precipitation dataset used in this study is from a network of 162 stations in NE China (Fig. 1; 35° – 55° N,

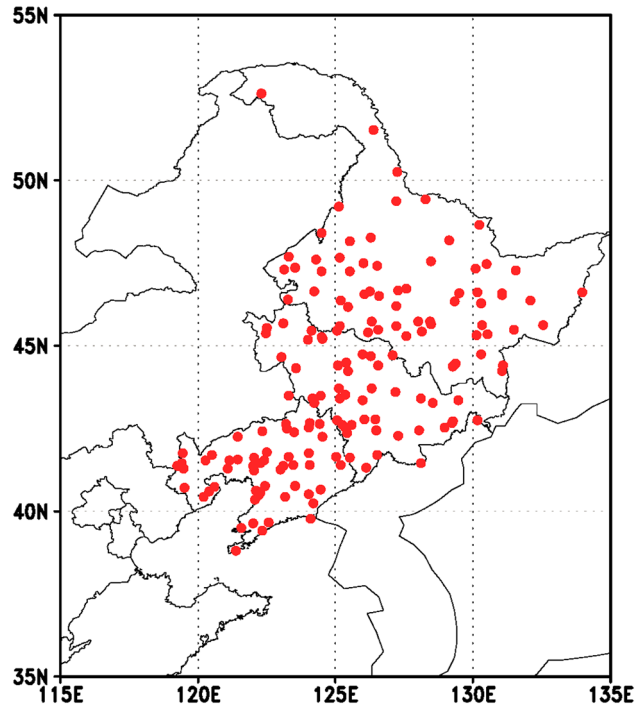


Fig. 1 Geographical location of the 162 observational stations used in this study

115°–135°E) for the period from January 1961 to December 2014, provided by the China Meteorological Administration. This dataset is much denser than that used in our previous work (Ying et al. 2015, 2017), which has only 15 stations in NE China. The monthly mean SSTs (on a 1.0° latitude × 1.0° longitude grid) used in this study are taken from the U.K. Met Office Hadley Center Sea Surface Temperature dataset (HADISST1.1; Rayner et al. 2003) for the same 54-year period. The monthly mean geopotential height field, the zonal and meridional wind field, and the specific humidity dataset (at 300, 400, 500, 600, 700, 850, 925 and 1000 hPa on a 2.5° latitude × 2.5° longitude grid), are from the National Centers for Environmental Prediction–National Center for Atmospheric Research (NCEP–NCAR) Reanalysis (Kalnay et al. 1996) for the same 54-year period.

2.2 Methods

Readers are referred to Zheng and Frederiksen (2004) and Frederiksen and Zheng (2007) for a detailed description of the underlying ideas and description of the methodology.

In the ZF2004 approach, the covariance matrix of the slow or predictable component and the intraseasonal or unpredictable component can be derived from the total interannual covariance, see the [Appendix](#) for more details. The potential predictability is estimated as the ratio of slow to total variance. Once the intraseasonal and slow covariance matrices of the seasonal mean precipitation have been estimated by the ZF2004 decomposition method, an empirical orthogonal function (EOF) analysis is applied to identify the leading modes of each covariance matrix. For convenience, we refer to the EOFs of the slow and intraseasonal covariance matrices as the predictable or slow modes (S-EOFs) and unpredictable or intraseasonal modes (I-EOFs), respectively, of interannual variability in the seasonal mean precipitation. The corresponding principal component (PC) time series of each predictable mode is obtained by projecting the field of seasonal mean

precipitation anomalies onto the corresponding EOF mode for each season and year in the time series.

3 Results

3.1 Potential predictability

We begin our study with an initial estimation of the potential predictability of seasonal mean precipitation in NE China during the period 1961–2014, using Eq. (9) in the [Appendix](#). Generally, the potential predictability of seasonal mean precipitation in NE China (expressed as the ratio of slow to total variance; S/T) is moderate for the seasons from January–February–March (JFM) to October–November–December (OND) (Table 1), with the highest value of 0.32 in June–August–September (JAS) and lowest value of 0.10 in April–May–June (AMJ). This indicates that the precipitation of NE China is mainly associated with intraseasonal variability. The spatial distribution of total variance and potential predictability of seasonal precipitation in NE China from JFM to OND are shown in Fig. 2. The NE China rainfall displays its largest amplitude and variability in the warm seasons (AMJ and JAS; Fig. 2b–c, f–g), consistent with the development of the East Asian summer monsoon. A similar northwest–southeast spatial gradient is generally apparent in the precipitation climatology and variability for all of the four seasons (Fig. 2a–h), probably due to the influence from the EAM and to topography. Unlike the total variance of seasonal precipitation over NE China, the maximum loadings of potential predictability are localized in a more limited area (Fig. 2i–l), which is consistent with the moderate predictability seen in Table 1. In particular, JAS has significantly larger potential predictability than other seasons in most of NE China; the largest predictability is seen in the south and north part of NE China during JFM, the southern part of NE China during AMJ, and the central part of NE China during OND. This indicates reasonable predictability in some regions.

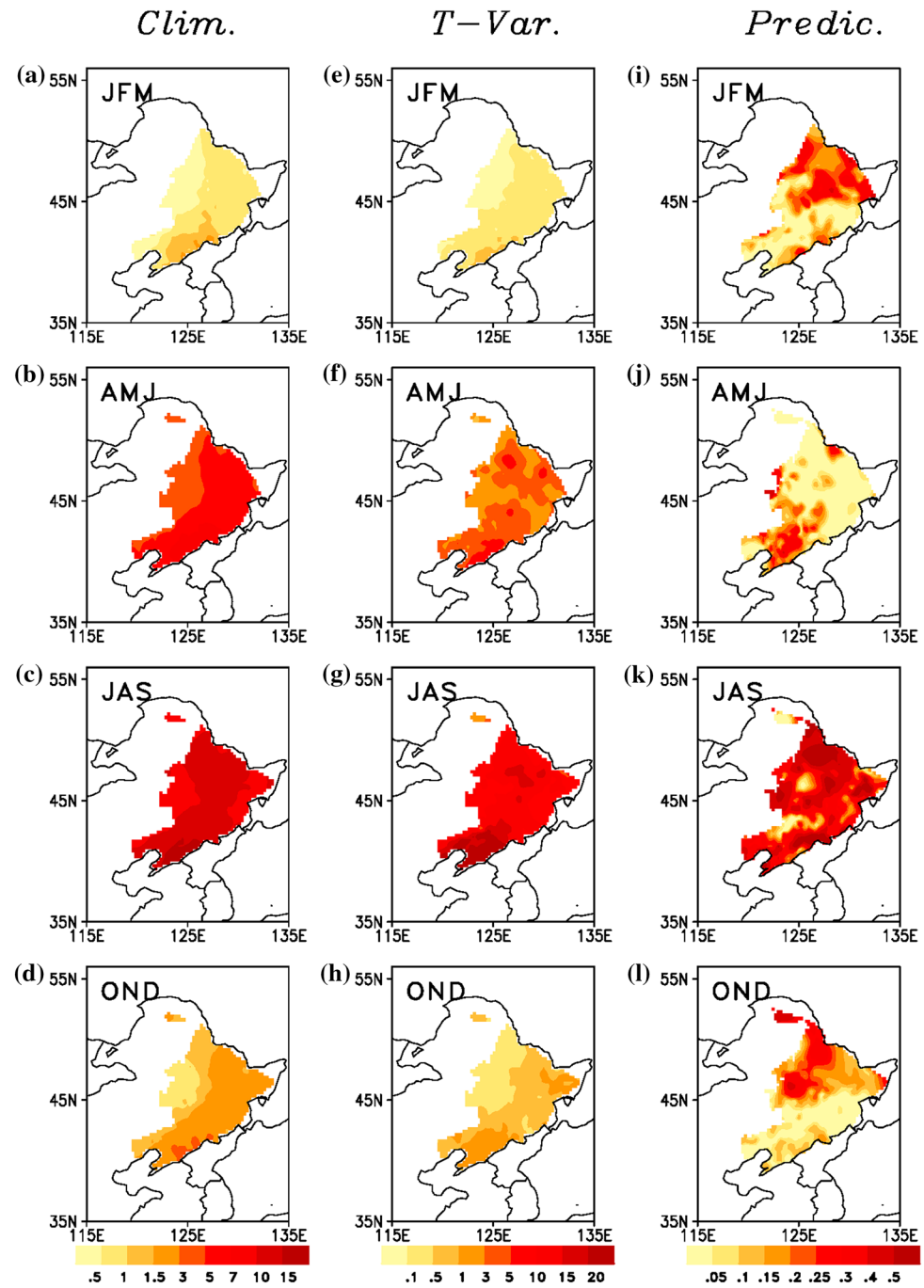
Table 1 Variability of the total, intraseasonal and slow component of the seasonal rainfall pattern (left three columns; units: mm²/month²), the potential predictability of seasonal mean precipitation (S/T; fourth

column), and the explained variance percentage of the PCs associated with the slow and the intraseasonal EOF precipitation modes

Season	Total Var	Intra Var	Slow Var	S/T	% Explained var.			
					S-PC1 (%)	S-PC2 (%)	I-PC1 (%)	I-PC2 (%)
JFM	3186	2677	509	0.16	63**	12	61	9
AMJ	55,870	50,285	5585	0.10	43	12	36	15
JAS	241,338	164,112	77,226	0.32	32	15	44	13
OND	13,030	11,471	1559	0.12	57*	9	48	14

S-PCs with significant linear trend are marked by: ** (at 5% level) and * (at 10% level)

Fig. 2 Spatial distributions of **a–d** the climatology mean (units: cm/month), **e–h** the total precipitation variance (units: $\text{cm}^2/\text{month}^2$) and **i–l** the potential predictability of seasonal precipitation over northeastern China for JFM, AMJ, JAS and OND during the period 1961–2014



As the intraseasonal variance is largely responsible for the interannual variance of seasonal precipitation in NE China, it is important to identify the patterns of interannual variability that arise from the slow (potentially predictable) and intraseasonal components separately, using the ZF2004 method. This could allow identification of the sources of the predictability of seasonal precipitation, and the sources of prediction uncertainty. Our discussion below focuses on the predictable and unpredictable EOF

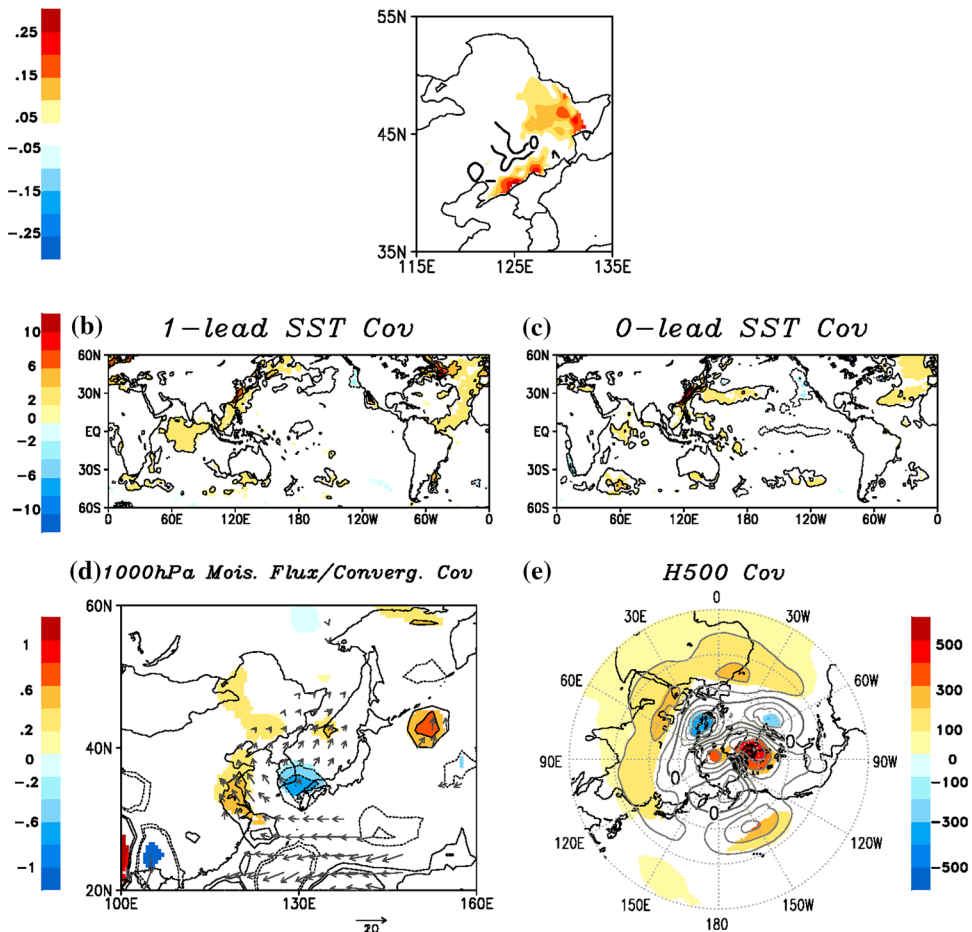
modes that explain the largest percentage of variance in each component.

3.2 Predictable patterns of interannual variability

In this section, the spatial distribution and temporal variation of the leading EOF modes for the predictable component of seasonal precipitation in NE China during JFM, AMJ, JAS and OND, respectively, are examined.

Possible SST predictors for these predictable precipitation modes are investigated by calculating the covariance between the PC time series of the predictable precipitation modes and the slow components of one-season-lead (e.g. the SST of AMJ and the precipitation PC of JAS) and simultaneous (e.g. the SST of JAS and the precipitation PC of JAS) seasonal mean SST anomalies, using Eq. (8) in the [Appendix](#). To aid with the physical interpretation of the predictable precipitation modes, we further examine the atmospheric circulation associated with the predictable precipitation modes. This is done by estimating the covariance between the S-PCs of predictable precipitation modes and the predictable component of the contemporary atmospheric fields (including the height field, moisture transport, and moisture convergence/divergence). It is important to note that the associated atmospheric circulation patterns are examined at different levels from the lower to the upper troposphere. However, we only show the circulation covariance maps at the levels with the larger covariance values. The statistical significance of the SST and circulation slow covariances are estimated using the Chi square test (see the [Appendix](#)).

Fig. 3 Spatial pattern of **a** the leading predictable precipitation mode, and the covariance between the PC time series for the predictable precipitation mode and the slow component of **b** the one-season-lead and **c** the contemporary SST (units: mm/month C), **d** the contemporary 1000-hPa moisture flux (units: mm/month g s kg⁻¹) and moisture convergence (units: 10⁻⁵ mm/month g s kg⁻¹ m⁻¹), and **e** the contemporary 500-hPa geopotential height (units: mm/month m), during JFM of 1961–2014. For the covariance maps, positive contours are solid and negative contours are dashed. The shaded areas and the vectors in the covariance maps are significant at the 95% confidence level, using the Chi-squared test



3.2.1 JFM

The leading predictable mode of seasonal mean precipitation for JFM, which explains 63% of the variance in the slow component, is presented in Fig. 3a. At the phase shown here, positive loadings correspond to wetter-than-normal conditions over NE China, with positive centers over the north and south of NE China. Recall that, in JFM, these are the regions that also have the largest predictability. The PC time series associated with the leading predictable modes of NE China precipitation in JFM shows an apparent increasing trend from 1961 to 2014, with statistical significance above the 95% level based on the Student's *t* test. This indicates the occurrence of a steep wetting trend over NE China during JFM. The trends for NE China precipitation anomalies was further examined using precipitation totals at each individual station during JFM 1961–2014, and the trend pattern is quite similar to the leading slow mode of JFM (figures not shown here). It is also consistent with the finding of Xiao et al. (2017; their Figs. 4, 5) and Gao et al. (2014b; their Fig. 3d), who found a wetting tendency present in

winter since the mid-1990s. Consistent with the latter, a comparison of the average amplitude of the JFM PC time series before and after 1995 indicates that the amplitude is higher on average in the latter period.

The one-season-lead and contemporary SST covariance maps associated with the leading predictable precipitation JFM modes are shown in Fig. 3b, c. Note that only those covariances that are statistically significant at the 95% level are shaded. The most consistent feature that appears in both the simultaneous and lead–lag SST covariance pattern is the region of significant positive values in the south of the Japan Sea and nearby regions, implying that the JFM predictable precipitation signals in NE China are largely associated with local SST variability. This is also consistent with the local circulation patterns with statistically significant positive 500-hPa geopotential height anomalies (an anticyclone) situated over the south of NE China, as shown in Fig. 3e. This anomalous anti-cyclone has the same phase in the lower, middle and upper troposphere (figures not shown), showing an equivalent barotropic structure in the entire troposphere. Along the western edge of the local anomalous anticyclone, the southwesterly wind in the lower troposphere brings moisture from the south to NE China (vector plots in Fig. 3d) and causes wetter-than-normal conditions in this area. We can also see from Fig. 3d that there is moisture convergence centered over NE China, which facilitates the precipitation pattern in this region.

Another notable feature in the one-season-lead and contemporary SST covariance maps is the significant positive anomalies in the North Atlantic, which suggests the North Atlantic SST may also be a possible source of predictability for the leading JFM precipitation mode. The linkage between the SSTs in the North Atlantic and the interannual variability of climate change in China (Wu et al. 2011; Jiang et al. 2014), the EAM (Zuo et al. 2012, 2013; Wang et al. 2010) and EAM rainfall (Gu et al. 2009) has also been noted in previous studies. The possible mechanisms through which the Atlantic Ocean influences NE China JFM precipitation may involve the impact of SST anomalies on local convection in the tropical Atlantic region and the consequent excitation of a Rossby wave train pattern response that propagates into the North Atlantic and the Eurasian continent in winter (Lu 2005; Zuo et al. 2013; Zhou and Wu 2015). Consistent with this idea, a zonal wave train pattern over the Atlantic–Eurasia region is clearly seen in the 500-hPa height covariance pattern associated with the leading JFM predictable mode (Fig. 3e). In particular, significant positive height anomalies prevail over both the sub-polar North Atlantic and Siberia, while significant negative height anomalies prevail over the North Atlantic, and western and eastern Eurasia.

3.2.2 AMJ

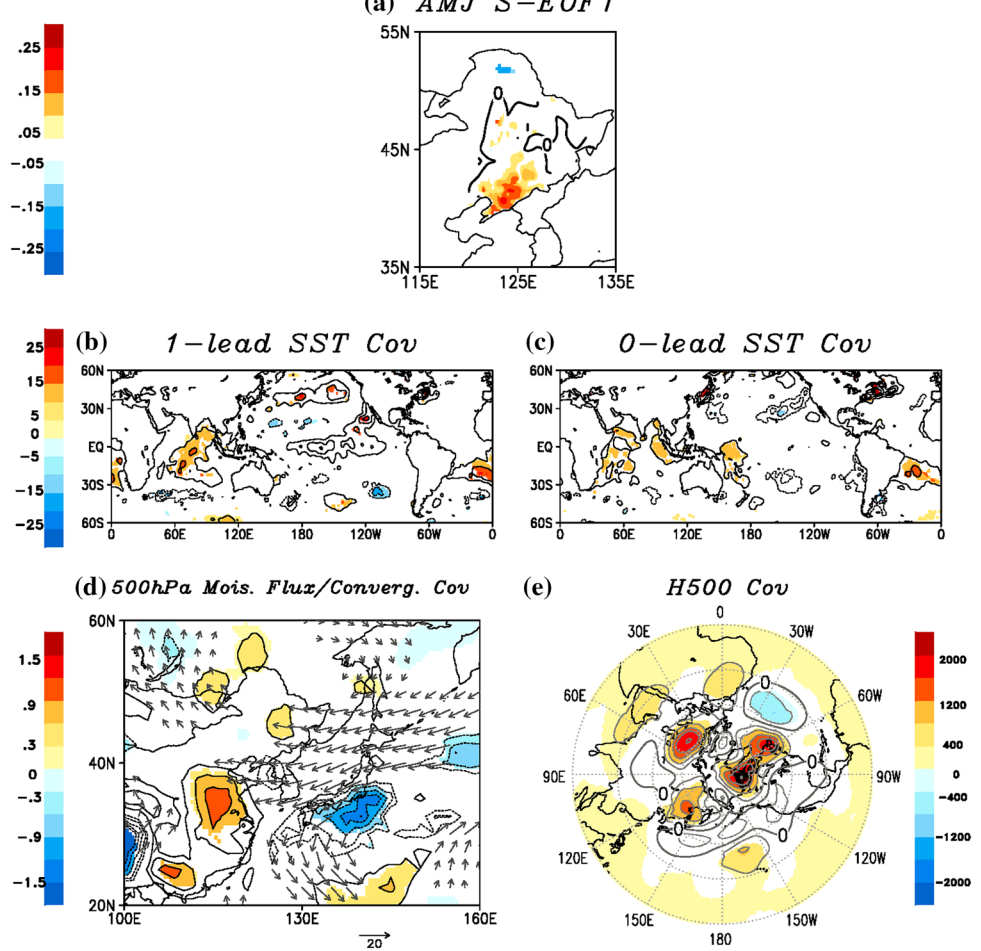
The leading predictable precipitation mode in NE China during AMJ, with an explained variance of 43% in the slow component, is shown in Fig. 4a. At the phase shown here, there are positive loadings centered over the south of NE China, corresponding to wet conditions in the region. The most obvious feature that appears in both the one-season-lead and contemporary SST covariance patterns is the maximum centered in the Indian Ocean (Fig. 4b, c). Again, covariances that are statistically significant at the 95% confidence level are shaded. This suggests that the Indian Ocean SST may be the predictability source of the leading predictable AMJ mode. In particular, when a warming takes place over the tropical Indian Ocean, the precipitation over the south of NE China is enhanced. Previous studies have explored the relationship between the Indian Ocean SST and the Asian monsoon and climate conditions in China extensively. For example, Gao et al. (2014b) found that the Indian Ocean SST in spring correlates significantly and positively with NE China precipitation in spring (their Fig. 7a), which is in agreement with our results.

When we examine the atmospheric circulation anomalies associated with the leading predictable mode during AMJ, we find that the corresponding 500-hPa geopotential height covariance associated with the leading predictable mode of AMJ (Fig. 4e) displays some amplitude over the Indian Ocean, which could be the teleconnection in the height response to Indian Ocean SST variability. Corresponding to the atmospheric circulation patterns, an anomalous anticyclonic circulation is located over NE China (Fig. 4e) and from the eastern edge of this anticyclone, more moisture is brought into NE China from the north (vector plots in Fig. 4d), resulting in anomalous moisture convergence over NE China (Fig. 4d) and responsible for the positive anomaly of the slow component of precipitation there.

3.2.3 JAS

The leading predictable precipitation mode for JAS is shown in Fig. 5a, for which the explained variance is 32% in the slow component. At the phase shown here, there are positive anomalies in NE China, with the maximum centers over southern NE China, corresponding to the wetter-than-normal conditions over this area. The associated lead–lag and contemporary SST covariance maps show similar characteristics, with statistically significant negative values in the eastern tropical Pacific Ocean (Fig. 5b, c). This indicates that the El Niño–Southern Oscillation (ENSO) is a possible SST predictor for the NE China precipitation variability during this season. Another notable feature in the contemporary SST covariance map is the significant

Fig. 4 As in Fig. 3, but for the leading predictable mode of AMJ, and the 500-hPa moisture flux and moisture convergence



covariance between NE China rainfall and the SSTs over the Indian Ocean and local area (Fig. 5c). Previous studies have also found a close relationship between the summer NE precipitation anomalies and the simultaneous local SST (Gao et al. 2014a).

The slow covariance of the 500-hPa geopotential height associated with the leading JAS precipitation mode (Fig. 5e) shows similar spatial structures to the summer Polar–Eurasia pattern (POLEUR), with positive height centers over the pole and negative anomalies over Eurasia, and has a pattern correlation of -0.51 with the canonical POLEUR [see, for example, http://www.cpc.ncep.noaa.gov/data/teledoc/poleur_map.shtml; Barnston and Livezey (1987)] for JAS. It is also similar to that of the POLEUR pattern of Zheng et al. (2008, S-EOF1 in their Fig. 3), but for JJA, which is significantly related to the SSTs over the Indian Ocean. Gao et al. (2016) examined the relationship between the teleconnection pattern of POLEUR and the atmospheric circulation conditions over Asia and the Pacific, and found that POLEUR exerts considerable control over westerlies and the persistent vortex over Asia in

summer, which could further result in precipitation anomalies over this area.

For the leading predictable mode of NE China precipitation during JAS, we are interested in the relationship between rainfall and the upper-level moisture conditions, taken here at 300 hPa. This is because the remote forcing from the eastern tropical Pacific plays an important role for this mode, and the largest rainfall–moisture correlations appear in the upper troposphere. The most significant feature in the covariance map of moisture flux associated with JAS S-EOF1 (Fig. 5d) is an anomalous anticyclone over the region of Japan and NE China. This anticyclonic center can also be observed in the slow covariance map of 500-hPa geopotential height (Fig. 5e), and it is even more statistically significant for a higher level of geopotential height at 300 hPa (not shown here). On the western edge of this anomalous anticyclone, the moisture over NE China is mainly transported from northern central China to NE China. Corresponding to these moisture transport conditions, large moisture convergence is situated over NE China, while the moisture divergence center is over

Fig. 5 As in Fig. 3, but for the leading predictable mode of JAS, and the 300-hPa moisture flux and moisture convergence

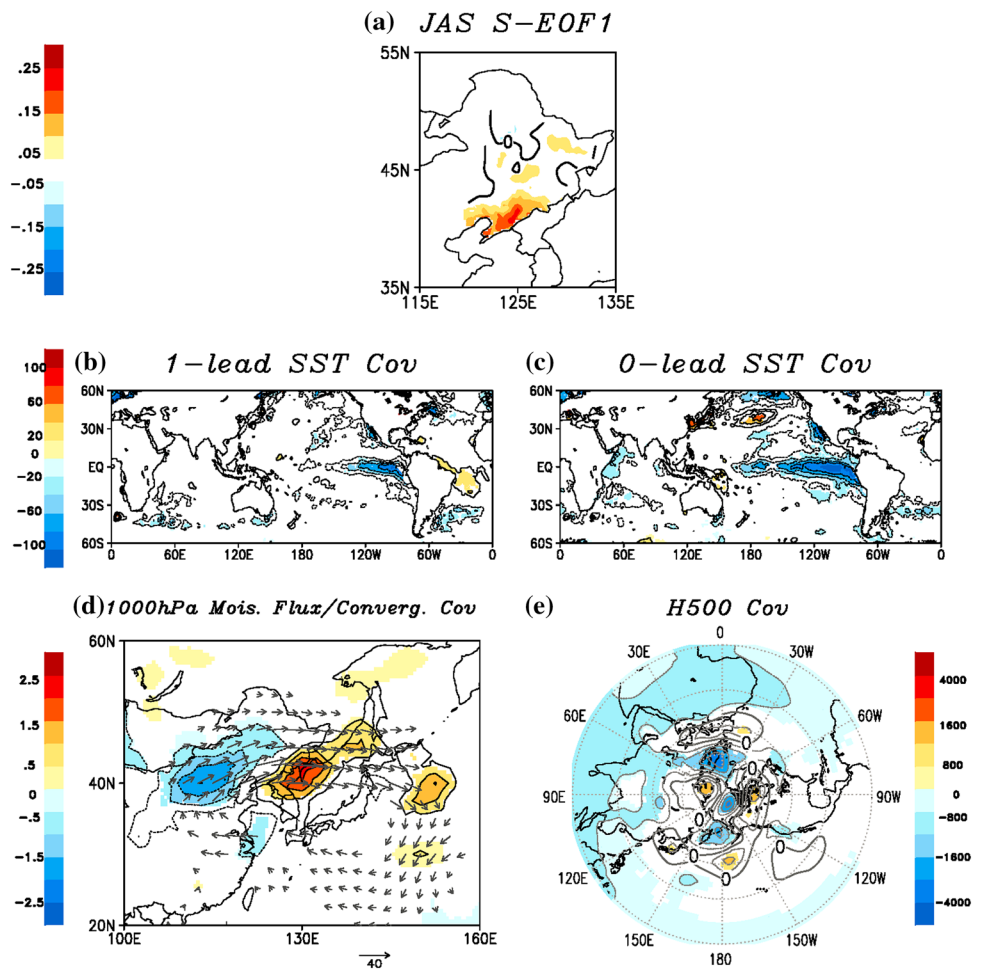
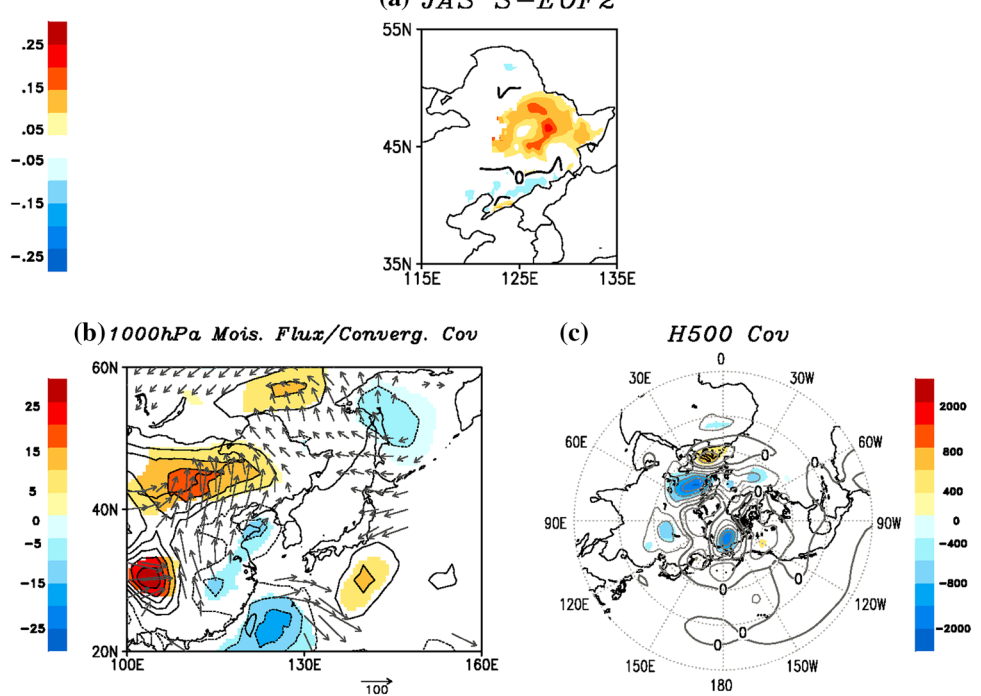


Fig. 6 a–c are the same as in Fig. 3a, d–e but for the second predictable mode of JAS



northern central China (Fig. 5d), responsible for the wetter-than-normal conditions in NE China.

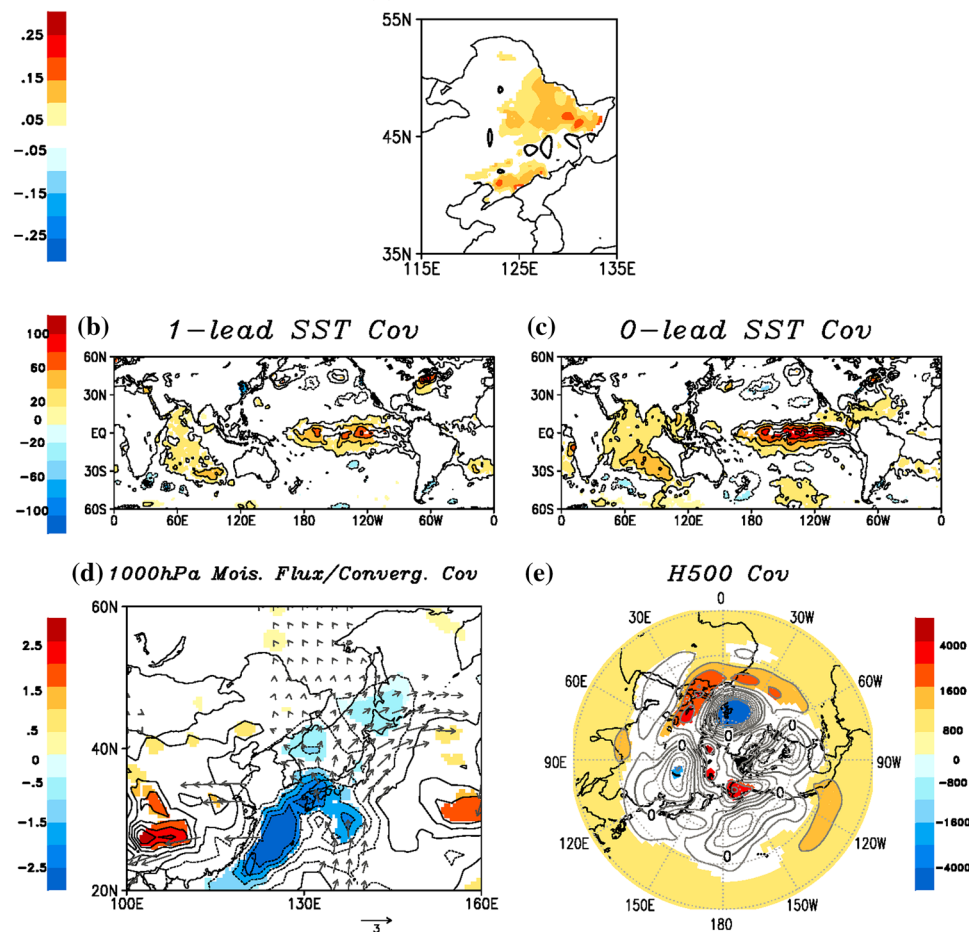
The second predictable rainfall mode during JAS, with an explained variance of 15%, is shown in Fig. 6a. For this particular phase, it is generally a wetter-in-the-north and drier-in-the-south dipole structure. When examining the slow covariance between this predictable mode and the global SSTs, there is barely any significant covariance (not shown here). The slow covariance of 500-hPa geopotential height associated with the second predictable JAS mode (Fig. 6c) shows a summer NAM-like zonal structure [see, for example, the S-EOF3 of Zheng et al. (2008) the pattern correlation with the canonical NAM for JAS is 0.63]. This implies a close connection between the second JAS predictable rainfall mode and the variability of the NAM. Previous studies have also revealed a linkage between the NAM and the interannual variability of China's climate (e.g. Gao et al. 2003; Li et al. 2008; Zhou and Li 2008; Zhu 2009; Gong et al. 2011; Zuo et al. 2015; Ying et al. 2015, 2016, 2017), in which the relationship has been found to exist during winter and summer. In addition, the North Atlantic Oscillation has been identified as a natural

mode of the climate system due predominantly to internal atmospheric dynamics, and has no significant SST predictors at the one-season lead time (Barnett 1985), which is generally consistent with our results. Figure 6b shows the slow covariance of the 1000 hPa moisture flux and convergence associated with the second predictable precipitation mode of JAS. There is an anomalous low centered over the Lake Baikal and an anomalous high centered over the north of Japan in both the slow covariance patterns of moisture flux (vector plots of Fig. 6b) and the 500-hPa geopotential height (Fig. 6c). As a result, more moisture is delivered to the northern part of NE China from the south, causing wetter-than-normal conditions there. We can also see from Fig. 6b that the moisture convergence situated in the north of NE China and the divergence in the south of NE China are facilitating the dipole rainfall pattern in this region.

3.2.4 OND

The leading predictable rainfall mode of OND, with an explained variance of 57%, is shown in Fig. 7a. The spatial structure of this precipitation mode shows positive

Fig. 7 As in Fig. 3, but for the leading predictable mode of OND, and the 300-hPa moisture flux, moisture convergence and geopotential height



loadings all over NE China, with maximum centers over north and south of NE China, corresponding to the wetter-than-normal conditions. The PC time series associated with the leading slow mode of OND shows a positive trend with 90% significant level. This indicates a wetting trend in OND precipitation, which is consistent with Xiao et al. (2017). The most obvious feature in both the one-season-lead and contemporary SST covariances maps is the significant positive values, corresponding to warming, over the eastern tropical Pacific Ocean and tropical Indian Ocean (Fig. 7b, c), which suggests the impact of ENSO on NE China precipitation variability during OND. Previous studies have also identified ENSO as a potential predictor for climate variability in China (e.g. Liang et al. 2009; Yang et al. 2008; Ying et al. 2013, 2015, 2017), through its influence on the western North Pacific heating and South Asian heating (e.g. Nitta 1987; Wang et al. 2000; Wu 2002).

The 300-hPa geopotential height covariance pattern associated with the ENSO-related predictable precipitation signals during OND is shown in Fig. 7e. The most remarkable feature in the mid-high latitudes is the presence of significant anomalous cyclonic centers over the area around Lake Baikal and the North Atlantic. Another noticeable feature in the 300-hPa height covariance associated with the leading predictable precipitation signal of OND is the occurrence of broad positive values all over the tropical region. This is the area most affected by the Hadley cell and the WPSH. In particular, when the Hadley cell circulation intensifies and the WPSH becomes stronger and extends anomalously more westward, there are wetter than normal conditions in NE China. The intensification of the NH winter Hadley cell was found to be associated with tropical SST variations and global warming (Quan et al. 2004a; Nguyen et al. 2013; Grainger et al. 2017). Previous studies also found that NE China climate is affected by the general circulation in both the tropics and extra-tropics during summer and winter, including the WPSH and large-scale circulation systems in the mid-high latitudes (e.g. Shen et al. 2011; Gao et al. 2014b; Ying et al. 2015). As a response to the joint sinking flow from an intensified Hadley cell, a stronger Ferrel cell occurs in the latitudes between 50° and 60°N, corresponding to an anomalous low over the mid-high latitudes. This atmospheric circulation pattern favors an anomalous southerly wind, which brings warm and moist air from the northwestern Pacific to NE China (vector plots in Fig. 7d), and causes moisture convergence and positive precipitation anomalies in this region (Fig. 7d).

3.3 Unpredictable patterns of interannual variability

As discussed in Sect. 3.1, the interannual variability of seasonal precipitation in NE China is largely related to the

intraseasonal component. So, in this section, we discuss the modes of interannual variability in this component, by applying an EOF analysis to the intraseasonal covariance matrix. Furthermore, we examine the associated atmospheric circulations. This is done to aid the physical interpretation of these intraseasonal precipitation modes, by estimating the covariance between the PC time series of the intraseasonal precipitation EOFs and the intraseasonal component of the atmospheric fields, using Eq. (3) in the [Appendix](#). The statistical significance of the intraseasonal covariances between the unpredictable precipitation modes and the atmospheric circulations are calculated using the Student's *t*-test (see the [Appendix](#) for more details).

The leading unpredictable modes of NE China precipitation from JFM to OND, which explain 61, 36, 44 and 48% of the explained variance in the intraseasonal component, respectively, are shown in Fig. 8a–d. Unlike the predictable precipitation modes in NE China, the spatial structure of the unpredictable modes do not change much between seasons. Specifically, in the phase shown here, there are positive loadings everywhere in NE China, corresponding to wet conditions in this region. The 500-hPa geopotential height associated with the leading predictable modes are shown in Fig. 8e–h. Note we only shade the areas with covariances at the 95% significant confidence level. In contrast with the largely zonally symmetric structure of the anomalous 500-hPa height associated with the predictable precipitation signals, a more wavy spatial structure can be seen for the unpredictable case. From JFM to JAS, a notable feature of the 500-hPa geopotential height is an anomalous low centered over Lake Baikal and an anomalous high centered over the south of Japan (Fig. 8 e–g), which is accompanied by anomalous southerlies (vector plot in Fig. 8a–c) that bring moisture to NE China and result in anomalously wetter-than-normal conditions there. Similar to JFM–JAS, the covariance pattern of the vertically integrated moisture flux associated with the OND I-EOF1 also shows a cyclonic anomalous center over NE China (Fig. 8d), which may explain the positive precipitation anomaly there. However, the covariance pattern of the 500-hPa geopotential height features some remote connections with the anomalous high in western Europe and the eastern Pacific (Fig. 8h), which may be attributable to the intraseasonal variability of ENSO (Frederiksen and Zheng 2004).

The spatial structure of the second unpredictable modes of NE China precipitation during JFM–OND, with explained variances of 9, 15, 13 and 14%, are presented in Fig. 8i–l. At the phase shown here, there are positive anomalies in the north of NE China and negative anomalies in the south. In JFM, a significant feature in the 500-hPa height covariance pattern is an anticyclonic center over the Okhotsk Sea (Fig. 8m), which brings the moist air from the Japan Sea to NE China (vectors in Fig. 8i) and

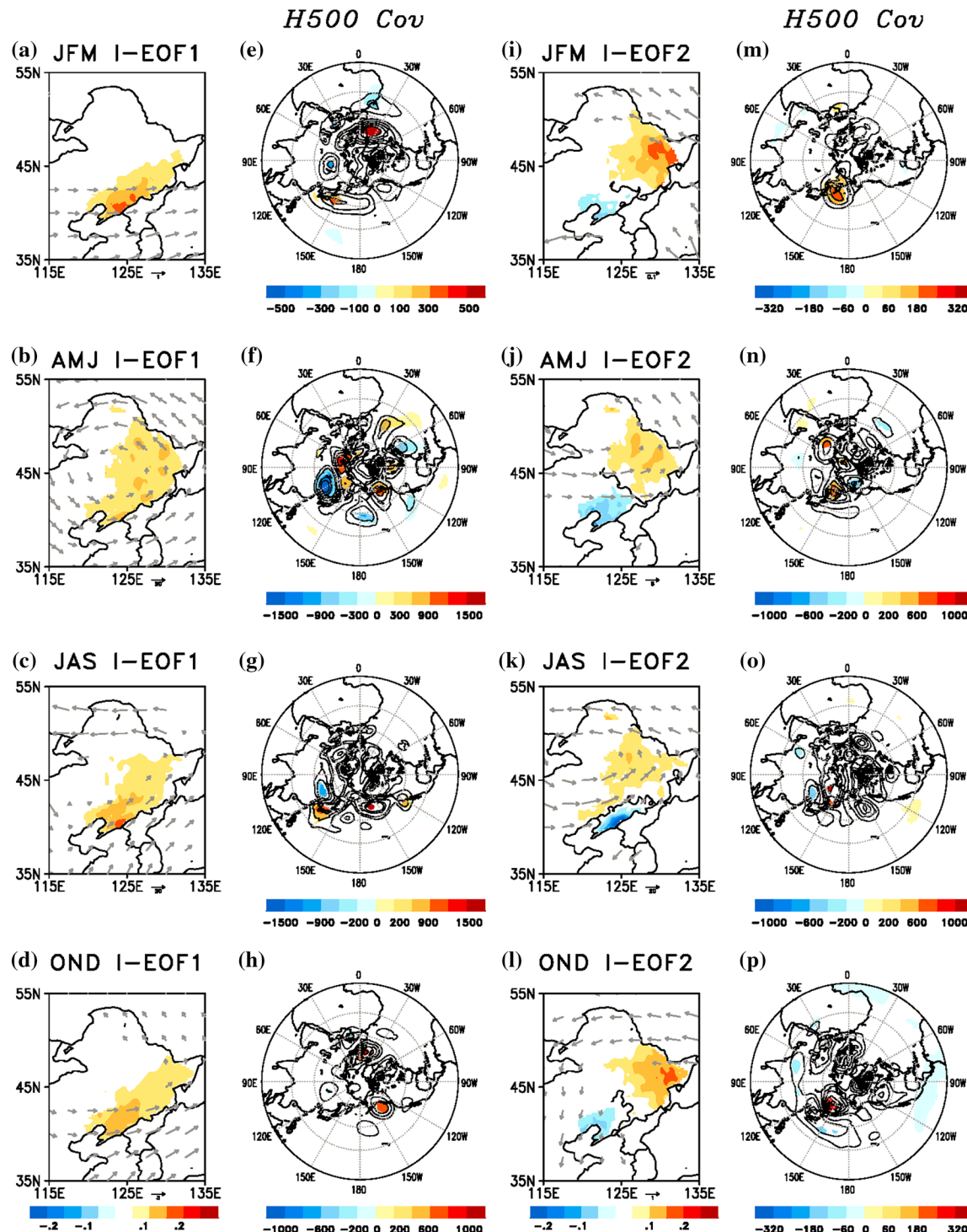


Fig. 8 Spatial patterns of **a–d** the first and **i–l** the second unpredictable precipitation modes and the covariance between the PC time series for the unpredictable precipitation mode and the intraseasonal component of the contemporary vertically integrated (at 300, 400, 500, 600, 700, 850, 925 and 1000 hPa) moisture flux (units: 10^3 mm/month $\text{kg m}^{-3} \text{s}^{-1}$), and the intraseasonal covariance maps of contemporary 500-hPa geopotential height (units: mm/month m) associated

with **e–h** the first and **m–p** the second unpredictable rainfall modes for JFM, AMJ, JAS and OND, respectively, during 1961–2014. For the 500 hPa height covariances, positive contours are *solid* and negative contours are *dashed*. The shaded areas and the vectors in the covariance maps are significant at the 95% confidence level, using the Student's *t*-test

results in anomalously wetter conditions in the north of NE China. Previous studies have also found that the blocking high conditions over the Sea of Okhotsk and Lake Baikal are favorable for suppressed rainfall in NE China (Sun et al. 1994; Shen et al. 2011). During AMJ–OND, the covariance patterns of the atmospheric circulations for all of these three seasons show similar characteristics, with an anomalous cyclone over NE China and south of Japan and an anomalous anticyclone over the Okhotsk Sea (Fig. 8n–p), causing wetter conditions mainly in the north part of NE China.

4 Conclusion and discussion

This study applies the ZF2004 variance decomposition method to identify the potentially more predictable signals and unpredictable modes of seasonal mean precipitation in NE China during the four seasons of JFM, AMJ, JAS and OND. The main results are as follows:

The potential predictability of seasonal mean precipitation in NE China, estimated by the ratio of the variance of the potentially predictable component to the variance of the total seasonal mean anomalies, is generally moderate. The potential predictability is highest in summer (JAS), with a value of 0.32, and lowest in spring (AMJ), with a value of 0.1. Compared with the spatial distribution of the total variances, the maximum centers of the potential predictability of NE China precipitation are localized in a more limited area, consistent with the moderate predictability there.

Possible sources of the potential predictability of the seasonal mean precipitation in NE China are examined. In particular, the SST anomalies around the area of the Japan Sea and over the North Atlantic are closely linked to the leading predictable precipitation mode of JFM; the Indian Ocean SST anomalies comprise a possible predictor for the leading predictable precipitation mode during AMJ; and ENSO is a possible predictor for the leading predictable precipitation mode during JAS and OND. It should be noted that possible mechanisms for the strong seasonality in the ENSO impact to the seasonal NE rainfall have not been fully understood yet. More detailed analysis is needed, which is beyond the scope of this study. The prolonged linear trend, which can be seen in the PC time series associated with the leading predictable precipitation mode during JFM and OND, may also serve as a source of predictability of seasonal precipitation over NE China. Analysis of the covariance of the anomalous atmospheric circulations associated with the predictable precipitation modes shows that the POLEUR and NAM teleconnection patterns are strongly related to the leading two predictable mode of JAS, respectively, and the Hadley cell circulation is closely related to the leading predictable mode of OND.

The leading unpredictable modes of seasonal precipitation over NE China during JFM–OND show a similar monopole spatial structure, while the second unpredictable precipitation modes display a similar north–south dipole structure. Atmospheric circulation associated with the unpredictable modes have wavy structures, reflecting the interannual variability of the seasonal average of intraseasonal events.

We also examine the leading EOF modes of total seasonal mean precipitation fields, without using the ZF2004 decomposition method. The results show that the leading total modes better resemble the leading unpredictable modes shown in this study (figures not shown), consistent with the moderate predictability of the seasonal precipitation in this area. The intraseasonal patterns are most influenced by the intraseasonal variability and blocking, and is essentially unpredictable on the interannual/supra-annual time scale. Consequently, when examining the total seasonal means, it may be harder to identify the predictable signals from SST and atmospheric circulations, or they may even be missed. With the variance decomposition method, it is possible to extract the potentially predictable component from the unpredictable noise. So we could focus on the leading EOFs of the predictable component. Also, in looking at the relationship of these slow EOFs with the SST and circulation, we estimate the covariance with the slow component in each case, thus maximizing the predictive characteristics of this relationship.

Previous studies have indicated that the relationship between ENSO and the climate variability of China may have undergone interdecadal change during recent decades, as a result of the change in the life cycle of an ENSO event (e.g. Chang et al. 2000; Ying et al. 2015), or change in the associated atmospheric circulation pattern (e.g. Quan et al. 2004b; Wang et al. 2008; Wu et al. 2010). Gao et al. (2014b) and Wu et al. (2010) have also suggested that the connection between ENSO and the climate of NE China seems to lack robustness, which may be due to the interdecadal change in the rainfall–ENSO relationship. In future work, we will further explore if there are any interdecadal changes between ENSO and the predictable signals of seasonal precipitation over NE China.

Acknowledgements We gratefully acknowledge the two anonymous reviewers for their constructive comments, which helped greatly in improving the quality of this manuscript. This work was done during the visit of KY in the School of Earth, Atmosphere and Environment, Monash University. The work was supported by the National Key R&D Program of China (2016YFA0600402) and National Natural Science Foundation of China (91325108, 91425304, 41675094, 41605066 and 41405090).

Appendix

Let x_{ym} represent sample monthly values, within a season, in month m ($m=1, 2, 3$) and in year y ($y=1, \dots, Y$, where Y is the total number of years). The annual cycle is firstly removed from the data. Following ZF2004 and Frederiksen and Zheng (2007), the monthly time series of each climate anomaly can be conceptually decomposed into two components consisting of a seasonal “population” mean and a residual departure from this mean, as

$$x_{ym} = \mu_y + \varepsilon_{ym}, \quad (1)$$

Here, μ_y is the seasonal population mean in year y , and ε_{ym} is a residual monthly departure of x_{ym} from μ_y and arises from intraseasonal variability. The vector $\{\varepsilon_{y1}, \varepsilon_{y2}, \varepsilon_{y3}\}$ is assumed to comprise a stationary and independent annual random vector with respect to year. Equation (1) implies that month-to-month fluctuations, or intraseasonal variability, arise entirely from $\{\varepsilon_{y1}, \varepsilon_{y2}, \varepsilon_{y3}\}$ (e.g., $(x_{y1} - x_{y2}) = \varepsilon_{y1} - \varepsilon_{y2}$). We represent an average taken over an independent variable (i.e., m or y) by replacing that variable subscript with “o”. With this notation, a seasonal mean can be expressed as

$$x_{yo} = \mu_y + \varepsilon_{yo}, \quad (2)$$

Suppose now that we have two climate variables x_{ym} and x'_{ym} that satisfy Eqs. (1) and (2). The interannual covariance of the intraseasonal component could be estimated as

$$\hat{V}(\varepsilon_{yo}, \varepsilon'_{yo}) \approx \hat{\sigma}^2(3 + 4\hat{\phi})/9, \quad (3)$$

where,

$$\hat{\sigma}^2 = \frac{a}{2(1 - \hat{\phi})}, \quad (4)$$

$$\hat{\phi} = \left(\frac{a + 2b}{2(a + b)} \right), \quad (5)$$

$$a = \frac{1}{2} \left\{ \frac{1}{Y} \sum_{y=1}^Y [x_{y1} - x_{y2}][x'_{y1} - x'_{y2}] + \frac{1}{Y} \sum_{y=1}^Y [x_{y2} - x_{y3}][x'_{y2} - x'_{y3}] \right\}, \quad (6)$$

$$b = \frac{1}{2} \left\{ \frac{1}{Y} \sum_{y=1}^Y [x_{y1} - x_{y2}][x'_{y2} - x'_{y3}] + \frac{1}{Y} \sum_{y=1}^Y [x_{y2} - x_{y3}][x'_{y1} - x'_{y2}] \right\}. \quad (7)$$

Then, the covariance matrix of the slow or predictable component can be derived from the total interannual covariance. In particular, the covariance between two slow or predictable components can be estimated as,

$$\hat{V}(\mu_y, \mu'_y) \approx \hat{V}(x_{yo}, x'_{yo}) - \hat{V}(\varepsilon_{yo}, \varepsilon'_{yo}), \quad (8)$$

where the total variances $V(x_{yo}, x'_{yo})$ can be calculated directly from two seasonal means. It is worth emphasizing that the difference between the total and the intraseasonal variances, in general, consists of not only the covariance between μ_y and μ'_y , but also their interaction terms with ε_{yo} and ε'_{yo} . In the case where the intraseasonal and slow components are independent, the residual covariance reduces to the covariance of the slow component. When this is not the case, $V(x_{yo}, x'_{yo}) - V(\varepsilon_{yo}, \varepsilon'_{yo})$ may still be better related to the covariance between the two slow components than is $V(x_{yo}, x'_{yo})$.

We define the *potential predictability* as the ratio between the variance of the predictable component and the variance of the total component; that is,

$$p = \frac{V(\mu_y)}{V(x_{yo})}. \quad (9)$$

This quantity represents the fraction remaining after the removal of the intraseasonal component from the total (Madden 1976; Zheng et al. 2000). The larger the value, the more closely the seasonal mean precipitation anomalies or the precipitation corresponding PC time series are related to external forcing and very low-frequency internal dynamics, and the more likely the seasonal mean precipitation or the precipitation PCs can be predicted.

The statistical significance of the covariance between the associated PC time series of the slow precipitation modes over NE China and the slow component of SST and atmospheric circulations (including height field, moisture flux and convergence, in Sect. 3.2) is able to be estimated through a Chi square test, with one degree of freedom,

$$\chi^2 = -2 \sum_{y=1}^Y (LH_{0,y} - LH_{A,y}), \quad (10)$$

where $LH_{0,y}$ and $LH_{A,y}$ are the log-likelihoods of the null hypotheses $\hat{V}(\mu_y, \mu'_y) = 0$ and the alternative hypotheses respectively, given the observations (x_{yo}, x'_{yo}) ; and they are calculated using the multivariate normal distribution assumption (see Wilks 2006; Grainger et al. 2017), with the zero means and the covariance matrices V_0 and V_A ,

$$V_0 = \begin{bmatrix} \hat{V}(x_{yo}, x_{yo}) & \hat{V}(x_{yo}, x'_{yo}) \\ \hat{V}(\varepsilon_{yo}, \varepsilon'_{yo}) & \hat{V}(x'_{yo}, x'_{yo}) \end{bmatrix}, \quad (11)$$

$$V_A = \begin{bmatrix} \hat{V}(x_{yo}, x_{yo}) & \hat{V}(x_{yo}, x'_{yo}) \\ \hat{V}(x_{yo}, x'_{yo}) & \hat{V}(x'_{yo}, x'_{yo}) \end{bmatrix}. \quad (12)$$

The significance of the intraseasonal covariances between two climate variables can be estimated by a Student's *t* test. The *t* statistic, with the degree of freedom of *Y*-2, for each pair of intraseasonal covariance is,

$$t = \frac{r}{\sqrt{\frac{1-r^2}{Y-2}}}, \quad (13)$$

$$r = \frac{\hat{V}(\varepsilon_{yo}, \varepsilon'_{yo})}{\sqrt{\hat{V}(\varepsilon_{yo}, \varepsilon_{yo}) \hat{V}(\varepsilon'_{yo}, \varepsilon'_{yo})}}. \quad (14)$$

here, *r* is an estimation of the correlation between the associated PC time series of the intraseasonal precipitation modes over NE China and the intraseasonal component of atmospheric circulations.

References

- Bai R (2001) Relations between the anomaly of sea surface temperature in the Atlantic and the precipitation in summer over Northeast China. *Mar Sci Bull* 20(1):23–29 (**in Chinese**)
- Barnett TP (1985) Variations in near-global sea level pressure. *J Atmos Sci* 42:478–501
- Barnston AG, Livezey RE (1987) Classification, seasonality and persistence of low-frequency atmospheric circulation patterns. *Mon Weather Rev* 115:1083–1126. doi:[10.1175/1520-0493\(1987\)115<1083:CSAPOL>2.0.CO;2](https://doi.org/10.1175/1520-0493(1987)115<1083:CSAPOL>2.0.CO;2)
- Bueh C, Shi N, Ji L, Wei J, Tao S (2008) Features of the EAP event on the medium- range evolution process and the mid- and high- latitude Rossby wave activities. *Chin Sci Bull* 53:610–623
- Chang CP, Zhang Y, Li T (2000) Interannual and interdecadal variations of the East Asian summer monsoon and tropical Pacific SSTs. Part II: meridional structure of the monsoon. *J Clim* 13:4326–4340
- Ding Y (1992) Summer monsoon rainfalls in China. *J Meteor Soc Jpn* 70:373–396
- Ding Y (1994) Monsoons over china. Kluwer Academic Publishers, The Netherlands
- Frederiksen CS, Zheng XG (2004) Variability of seasonal-mean fields arising from intraseasonal variability: part 2, application to NH winter circulations. *Clim Dyn* 23:193–206
- Frederiksen CS, Zheng X (2007) Coherent patterns of interannual variability of the atmospheric circulation: the role of intraseasonal variability. In: Denier J, Frederiksen JS (eds) Frontiers in turbulence and coherent structures, World scientific lecture notes in complex systems, vol 6. World Scientific, Singapore, pp 87–120
- Gao H, Xue F, Wang H (2003) Influence of interannual variability of Antarctic oscillation on Meiyu along the Yangtze and Huaihe River valley and its importance to prediction. *Chin Sci Bull* 48(Supp. II):61–67
- Gao Z, Hu Z, Zhu J, Yang S, Zhang R, Xiao Z, Jha B (2014a) Variability of summer rainfall in Northeast China and its connection with spring rainfall variability in the Huang-Huai Region and Indian Ocean SST. *J Clim* 27:7086–7101. doi:[10.1175/JCLI-D-14-00217.1](https://doi.org/10.1175/JCLI-D-14-00217.1)
- Gao Z, Hu Z, Jha B, Yang S, Zhu J, Shen B, Zhang R (2014b) Variability and predictability of Northeast China climate during 1948–2012. *Clim Dyn* 43:787–804. doi:[10.1007/s00382-013-1944-0](https://doi.org/10.1007/s00382-013-1944-0)
- Gao T, Yu J, Paek H (2016) Impacts of four northern-hemisphere teleconnection patterns on atmospheric circulations over Eurasia and the Pacific. *Theor Appl Climatol*. doi:[10.1007/s00704-016-1801-2](https://doi.org/10.1007/s00704-016-1801-2)
- Gong Q, Wang H, Wang P (2006) Analysis of climate and anomaly features of summer precipitation in Northeast China. *Meteorol Sci Tech* 34:387–393 (**in Chinese**)
- Gong D, Yang J, Kim S-J, Gao Y, Guo D, Zhou T, Hu M (2011) Spring Arctic Oscillation-East Asian summer monsoon connection through circulation changes over the western North Pacific. *Clim Dyn* 37(11–12):2199–2216
- Grainger S, Frederiksen CS, Zheng X (2013) Modes of interannual variability of Southern Hemisphere atmospheric circulation in CMIP3 models: assessment and projections. *Clim Dyn* 41:479–500
- Grainger S, Frederiksen C, Zheng X (2014) Assessment of modes of interannual variability of southern hemisphere atmospheric circulation in CMIP5 models. *J Clim* 27:8107–8125
- Grainger S, Frederiksen C, Zheng X (2017) Projections of Southern Hemisphere atmospheric circulation interannual variability. *Clim Dyn* 48:1187–1211
- Gu W, Li C, Wang X, Zhou W, Li W (2009) Linkage between meiyu precipitation and North Atlantic SST on the decadal timescale. *Adv Atmos Sci* 26(1):101–108
- Han T, Chen H, Wang H (2015) Recent changes in summer precipitation in Northeast China and the background circulation. *Int J Climatol* 35:4210–4219. doi:[10.1002/joc.4280](https://doi.org/10.1002/joc.4280)
- He J, Wu Z, Qi L (2006) Relationships among the Northern Hemisphere annual mode, the Northeast Cold Vortex and the summer rainfall in Northeast China. *J Meteor Environ* 22(1):1–5 (**in Chinese**)
- Hu Z, Yang S, Wu R (2003) Long-term climate variations in China and global warming signals. *J Geophys Res* 108(D19):4614. doi:[10.1029/2003JD003651](https://doi.org/10.1029/2003JD003651)
- Jia X, Wang Q, Zhou N (2003) Analysis of climate features of precipitation anomalies in Northeast China in recent 50 years. *J Nanjing Inst Meteorol* 26:164–171 (**in Chinese**)
- Jiang Z, Yang H, Liu Z, Wu Y, Wen N (2014) Assessing the influence of regional SST modes on the winter temperature in China: the effect of tropical Pacific and Atlantic. *J Clim* 27:868–879
- Kalnay E, Kanamitsu M, Kistler R, Collins W, Deaven D, Gandin L, Iredell M, Saha S, White G, Woollen J, Zhu Y, Leetmaa A, Reynolds R, Chelliah M, Ebisuzaki W, Higgins W, Janowiak J, Mo KC, Ropelewski C, Wang J, Jenne R, Joseph D (1996) The NCEP/NCAR 40-year reanalysis project. *Bull Am Meteorol Soc* 77:431–471
- Li J, Yu R, Zhou T (2008) Teleconnection between NAO and climate downstream of the Tibetan Plateau. *J Clim* 21(8):4680–4690
- Liang JY, Ang S, Hu Z-Z, Huang BH, Kumar A, Zhang ZQ (2009) Predictable patterns of the Asian and Indo-Pacific summer precipitation in the NCEP CFS. *Clim Dyn* 32:989–1001
- Liang L, Li L, Liu Q (2011) Precipitation variability in Northeast China from 1961 to 2008. *J Hydrol* 404:67–76
- Lu R (2005) Impact of Atlantic sea surface temperatures on the warmest global surface air temperature of 1998. *J Geophys Res* 110:D05103. doi:[10.1029/2004JD005203](https://doi.org/10.1029/2004JD005203)
- Madden RA (1976) Estimates of the natural variability of time averaged sea-level pressure. *Mon Weather Rev* 104:942–952
- Nguyen H, Evans A, Lucas C, Smith I, Timbal B (2013) The Hadley Circulation in reanalyses: climatology, variability, and change. *J Clim* 26:3357–3376

- Nitta T (1987) Convective activities in the tropical western Pacific and their impacts on the Northern Hemisphere summer circulation. *J Meteorol Soc Jpn* 65:373–390
- Quan XW, Diaz HF, Hoerling MP (2004a) Change of the tropical hadley cell since 1950. In: Diaz HF, Bradley RS (eds) *Hadley circulation: past, present, and future*. Cambridge University Press, New York, pp 85–120
- Quan XW, Webster PJ, Moore AM, Chang H-R (2004b) Seasonality in SST forced atmospheric short-term climate predictability. *J Clim* 17:3090–3180
- Rayner NA, Parker DE, Folland CK, Alexander LV, Horton EB, Rowell DP (2003) Globally complete analyses of sea-surface temperature, sea-ice and marine air temperature, 1871–2000. *J Geophys Res* 108:4407
- Shen B, Lin Z, Lu R, Lian Y (2011) Circulation anomalies associated with interannual variation of early- and late-summer precipitation in Northeast China. *Sci China. Earth Sci* 54:1095–1104. doi:[10.1007/s11430-011-4173-6](https://doi.org/10.1007/s11430-011-4173-6)
- Song F, Zhou T (2014) Interannual variability of East Asian summer monsoon simulated by CMIP3 and CMIP5 AGCMs: Skill dependence on Indian Ocean–western Pacific anticyclone teleconnection. *J Clim* 27:1679–1697. doi:[10.1175/JCLI-D-13-00248.1](https://doi.org/10.1175/JCLI-D-13-00248.1)
- Sun L, Zhen XY, Wang Q (1994) The climatological characteristics of Northeast cold vortex in China. *Quart J Appl Meteor* 5:297–303 (**Chinese with English abstract**)
- Tang Y, Wang H, Yan D, Wang S (2005) Research on the spatial-temporal differentiation of precipitation in Northeast China in recent 50 years. *Sci Geogr Sin* 25:172–176 (**in Chinese**)
- Wang B, Linho (2002) Rainy season of the Asian-Pacific summer Monsoon. *J Clim* 15:386–398
- Wang B, Wu R, Fu X (2000) Pacific-East Asian teleconnection: How does ENSO affect East Asian climate? *J Clim* 13:1517–1536
- Wang B, Yang J, Zhou TJ, Wang B (2008) Interdecadal changes in the major modes of Asian–Australian Monsoon variability: strengthening relationship with ENSO since late 1970s. *J Clim* 21:1771–1789
- Wang B, Wu Z, Chang CP, Liu J, Li J, Zhou T (2010) Another look at interannual-to-interdecadal variations of the East Asian Winter Monsoon: the northern and southern temperature modes. *J Clim* 23:1495–1512
- Wilks DS (2006) Statistical methods in the atmospheric sciences. Academic Press, San Diego, p 648
- Wu R (2002) A mid-latitude Asian circulation anomaly pattern in boreal summer and its connection with the Indian and east Asian summer monsoons. *Int J Climatol* 22:1879–1895. doi:[10.1002/joc.845](https://doi.org/10.1002/joc.845)
- Wu R, Hu Z, Kirtman B (2003) Evolution of ENSO-related rainfall anomalies in East Asia. *J Clim* 16:3742–3758
- Wu R, Yang S, Liu S, Sun L, Lian Y, Gao Z (2010) Changes in the relationship between Northeast China summer temperature and ENSO. *J Geophys Res* 115:D21107. doi:[10.1029/2010JD014422](https://doi.org/10.1029/2010JD014422)
- Wu R, Yang S, Liu S, Sun L, Lian Y, Gao Z (2011) Northeast China summer temperature and North Atlantic SST. *J Geophys Res* 116:D16116. doi:[10.1029/2011JD015779](https://doi.org/10.1029/2011JD015779)
- Xiao M, Zhang Q, Singh VP (2017) Spatiotemporal variations of extreme precipitation regimes during 1961–2010 and possible teleconnections with climate indices across China. *Int J Climatol* 37:468–479. doi:[10.1002/joc.4719](https://doi.org/10.1002/joc.4719)
- Yang S, Yoo S-H, Yang R, Mitchell KE, van den Dool H, Higgins W (2007a) Response of seasonal simulations of a regional climate model to high-frequency variability of soil moisture during the summers of 1988 and 1993. *J Hydrometeor* 8:738–757. doi:[10.1175/JHM616.1](https://doi.org/10.1175/JHM616.1)
- Yang J, Liu Q, Xie S, Liu Z, Wu L (2007b) Impact of the Indian Ocean SST basin mode on the Asian summer monsoon. *Geophys Res Lett* 34:L02708. doi:[10.1029/2006GL028571](https://doi.org/10.1029/2006GL028571)
- Yang S, Zhang ZQ, Kousky VE, Higgins RW, Yoo S-H, Liang JY, Fan Y (2008) Simulations and seasonal prediction of the Asian summer monsoon in the NCEP Climate Forecast System. *J Clim* 21:3755–3775
- Ying K, Zheng X, Quan XW, Frederiksen CS (2013) Predictable signals of seasonal precipitation in the Yangtze-Huaihe river valley. *Int J Climatol* 33:3002–3015. doi:[10.1002/joc.3644](https://doi.org/10.1002/joc.3644)
- Ying K, Zhao T, Quan XW, Zheng X, Frederiksen CS (2015) Interannual variability of autumn to spring seasonal precipitation in eastern China. *Clim Dyn* 45(1–2):253–271
- Ying K, Zhao T, Zheng X, Quan XW, Frederiksen CS, Li M (2016) Predictable signals in seasonal mean soil moisture simulated with observation-based atmospheric forcing over China. *Clim Dyn* 47:2373–2395. doi:[10.1007/s00382-015-2969-3](https://doi.org/10.1007/s00382-015-2969-3)
- Ying K, Zheng X, Zhao T, Frederiksen CS, Quan XW (2017) Identifying the predictable and unpredictable patterns of spring-to-autumn precipitation over eastern China. *Clim Dyn* 48(9):3183–3206. doi:[10.1007/s00382-016-3258-5](https://doi.org/10.1007/s00382-016-3258-5)
- Zhao D, Zheng D, Wu S, Wu Z (2007) Climate changes in Northeastern China during last four decades. *Chin Geogr Sci* 17(4):317–324. doi:[10.1007/s11769-007-0317-1](https://doi.org/10.1007/s11769-007-0317-1)
- Zheng X, Frederiksen CS (1999) Validating interannual variability in an ensemble of AGCM simulations. *J Clim* 12:2386–2396
- Zheng X, Frederiksen CS (2004) Variability of seasonal-mean fields arising from intraseasonal variability: part 1. Methodology. *Clim Dyn* 23:171–191
- Zheng X, Frederiksen CS (2006) A study of predictable patterns for seasonal forecasting of New Zealand rainfall. *J Clim* 19:3320–3333
- Zheng X, Nakamura H, Renwick J (2000) Potential predictability of seasonal means based on monthly time series of meteorological variables. *J Clim* 13:2591–2604
- Zheng X, Straus DM, Frederiksen CS (2008) Variance decomposition approach to the prediction of the seasonal mean circulation: comparison with dynamical ensemble prediction using NCEP's CFS. *Q J R Meteorol Soc* 134:1997–2009
- Zhou T, Li J (2008) Climate change in China congruent with the linear trends of the annular modes. *Atmos Ocean Sci Lett* 1:1–7
- Zhou LT, Wu R (2015) Interdecadal variability of winter precipitation in Northwest China and its association with the North Atlantic SST change. *Int J Climatol* 35:1172–1179. doi:[10.1002/joc.4047](https://doi.org/10.1002/joc.4047)
- Zhu YL (2009) The Antarctic oscillation-East Asian summer monsoon connections in NCEP-1 and ERA-40. *Adv Atmos Sci* 26(4):707–716
- Zong H, Chen L, Zhang Q (2010) The instability of the interannual relationship between ENSO and the summer rainfall in China. *Chin J Atmos Sci* 34(1):184–192 (**Chinese**)
- Zuo J, Li W, Ren H, Chen L (2012) Change of the relationship between spring NAO and East Asian summer monsoon and its possible mechanism. *Chin J Geophys* 55:23–34 (**in Chinese**)
- Zuo J, Li W, Sun C, Xu L, Ren H (2013) Impact of the North Atlantic Sea surface temperature Triple on the East Asian summer Monsoon. *Adv Atmos Sci* 30(4):1173–1186
- Zuo J, Ren H-L, Li W (2015) Contrasting impacts of the Arctic oscillation on surface air temperature anomalies in Southern China between Early and Middle-to-Late Winter. *J Clim* 28:4015–4026